Chemical Engineering Journal 164 (2010) 410–417

Contents lists available at ScienceDirect

Chemical Engineering Journal

journal homepage: www.elsevier.com/locate/cej

Predicting the pressure distribution during roll compaction from uniaxial compaction measurements

B.A. Patel[a,b], M.J. Adams[a], N. Turnbull[b], A.C. Bentham[b], C.-Y. Wu[a,*]

[a] School of Chemical Engineering, University of Birmingham, Edgbaston, Birmingham, B15 2TT, UK
[b] Pfizer Ltd, Global Research and Development, Sandwich, Kent, CT13 9NJ, UK

ARTICLE INFO

Article history:
Received 13 October 2009
Received in revised form
13 December 2009
Accepted 14 December 2009

Keywords:
Roll compaction
Granulation
Compressibility
Uniaxial compression
Agglomeration
Johanson theory
Microcrystalline cellulose

ABSTRACT

The accuracy of predicting the pressure distribution in a roll compaction process using confined uniaxial compaction was assessed using microcrystalline cellulose (MCC, Avicel-PH102) as a model pharmaceutical powder. This involved an instrumented roll press and a range of roll gaps and roll speeds. The measured pressure-displacement data were described using the Johanson equation and a comparison was made with data obtained from uniaxial compaction. In addition, an existing uniaxial compression relationship was adapted to describe the data with the advantage that it can be applied to the whole pressure range especially at the lower pressure range. It has been shown that the predicted maximum pressure values using uniaxial compaction data are generally less than those measured. This was attributed to the more complex powder flow field in roll compaction compared to uniaxial compaction, which leads to (1) a non-uniform pressure distribution across the roll width with the pressure in the centre of the roll width being greater than the mean value and (2) a shear component of the flow field, and even the formation of shear band when the roll gap is small. Despite the differences between the measured and predicted pressure distributions, it is believed that uniaxial compaction is a useful method for screening different formulations in terms of ranking their expected performance in roll compaction.

1. Introduction

Most pharmaceutical tablets cannot be manufactured by direct compression of the formulation because of poor flowability and high segregation tendency. Consequently, the feed powders are usually granulated before tabletting. This has commonly involved the use of liquid binders through wet granulation. However, currently there is a growing interest in the use of dry granulation based on roll compaction (RC), which is a continuous process that has been used in the pharmaceutical industry for more than 50 years [1]. This is because it has the distinctive advantage that a liquid binder and additional heating are not required so that it can be used to process moisture, solvent or heat sensitive formulations. However, due to the complex nature of the processing conditions and the diversity of formulations used in the pharmaceutical industry, such issues as optimisating of the processing conditions and scale up are still not fully understood.

During roll compaction, the feed powder is compacted in the gap between two counter rotating rolls. As illustrated in Fig. 1, the process is usually divided into three regions [1–3]: (1) the *feed (slip) region* in which the stresses are small and densification is primarily due to particle rearrangement; (2) the *nip region* in which the particles deform plastically and/or fragment and in which a no-slip wall boundary condition applies; (3) the *exit region* that corresponds to an increase in the roll gap. The nip region is characterised by the nip angle, α (see Fig. 1), it is in this region that the powder is primarily consolidated into a coherent compact. The nip angle is defined with reference to the neutral angle γ, which is the angular position corresponding to the maximum pressure; this does not always occur at the minimum roll gap, e.g. Refs. [2]. A coherent ribbon is normally produced in the exit region that is subsequently milled to form granules. The thickness of a ribbon is invariably greater than the minimum roll gap because of the recovery of stored elastic strains that increase with increasing roll speed since there is less time for stress relaxation to occur.

Johanson [3] developed an analytical model of roll compaction that depends on the roll dimensions, the behaviour of the feed powder and the operating conditions. The calculation of the pressure distribution in the nip region is based on describing the compaction of the powder by an empirical uniaxial relationship. The pressure distribution is derived by segmenting this region into volumetric elements that are parallel to the centre-to-centre axis of the rolls. The stress at a given location is determined by the corresponding compressive strain. He also derived a method for calculating the nip angle based on a powder yield criterion. Nominally, the model allows the roll pressure distributions to be fitted accurately at pres-

* Corresponding author. Tel.: +44 121 4145365; fax: +44 121 4145324.
E-mail address: C.Y.Wu@bham.ac.uk (C.-Y. Wu).

1385-8947/$ – see front matter © 2009 Elsevier B.V. All rights reserved.
doi:10.1016/j.cej.2009.12.022

Nomenclature

c	microscopic pressure coefficient
D	roll diameter
h	current powder bed height
h_i	initial height of powder bed (UC)
h_α	height of powder bed corresponding to Σ_α (UC)
S^*	dimensionless roll gap (S/D)
S	roll gap
S_α	roll separation distance at angle α (RC)
S_β	roll separation distance at angle β (RC)
V_θ	volume of slab at angle θ
W	roll width
α	apparent nip angle
β	true nip angle
δ_E	effective angle of friction
γ	neutral angle
ε	actual compressive strain
$\tilde{\varepsilon}$	approximate compressive natural strain
θ	angular position
κ	compressibility constant for RC
K	compressibility constant for UC
ρ	current density
ρ_α	stress at Σ_α
σ_α	Johanson parameter determined by RC
$\hat{\sigma}_\alpha$	compressive stress parallel to centre-to-centre axis at α
Σ_α	Johanson parameter determined by UC
σ_θ	local roll pressure at θ
$\hat{\sigma}_\theta$	compressive stress parallel to centre-to-centre axis at θ
τ_0	mechanical strength
ϕ	wall friction angle

sures greater than some minimum provided that the nip angle is measured directly [3–5]. However, Bindumadhavan et al. [5] highlighted the sensitivity of the model to the peak pressure. Funakoshi et al. [1] and Miller [6] argued that there are a number of additional factors that must be considered for describing the performance of a roll compaction process including: (i) adequate powder needs to be conveyed to the slip region; (ii) the powder in the slip region must be conveyed completely to the minimum roll gap; (iii) the compaction pressure should be uniformly distributed over the nip region and (iv) vacuum de-aeration must be optimal before the nip region.

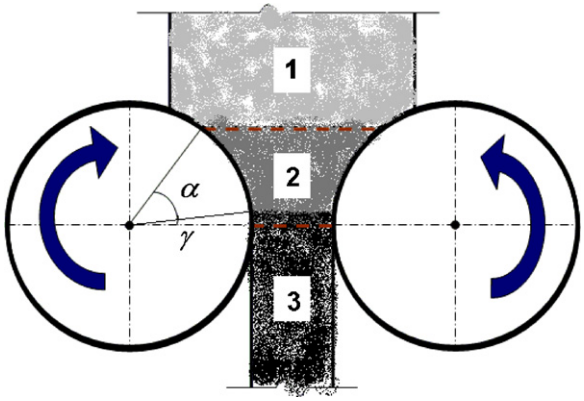

Fig. 1. Schematic representation of the roller compaction process. (1) Feed (slip) region; (2) nip region; (3) exit region.

Due to the complexity of compaction processes, most work has been carried out to characterise the physico-mechanical properties of compacts and to correlate powder behaviour during roll compaction with uniaxial compaction [7–11]. Using an instrumented roll compactor and a universal material testing machine, Michel [12] and Perrea [13] showed that the pressure/density relationship for aluminum powders during roll compaction is similar to that in uniaxial compaction, i.e., a similar packing density can be obtained for a given compression pressure during roll and uniaxial compaction. This was further confirmed recently by Miguelez-Moran [14] using a pharmaceutical powder, MCC Avicel-PH102. However, Miguelez-Moran et al. [14] emphasized that the same density could be reached at the same maximum compression pressure only if the tablet and the ribbon had the same thickness, so that the degree of deformation and the effect of wall frictions in both cases are similar.

Zinchuk et al. [15] developed a method for simulating roll compaction by uniaxial compaction using a compaction simulator, in which the movement of the top and bottom punches were specified to model the movement of a given point on the roll surface during roll compaction. They examined the solid fractions and tensile strength of real ribbons and simulated ribbons (i.e., tablets produced with the compaction simulator) and found that similar compression behaviour and equivalent tensile strengths were obtained when the real and simulated ribbons were compacted to the same solid fractions. Gupta et al. [7] explored the effects of ambient moisture on the compaction behaviour of MCC (Avicel-PH102) powder by making ribbons using both processes and measuring the Young's modulus, tensile strength and relative density. They found that increasing the moisture content of the feed powder resulted in a decrease in tensile strength. However, for ribbons produced by uniaxial compaction, they observed that increasing the moisture content increased the tensile strength. This was attributed to the difference in the thicknesses of the compacts produced by each process. During roll compaction the thickness of the compact is constrained by the roll gap whereas, for the uniaxial compaction, the thickness is controlled by the applied pressure. The thickness of a ribbon is related to the porosity and the strength is extremely sensitive to this parameter. However, Farber et al. [16] examined the strengths of tablets made directly from the blends and those made from milled ribbons. A model was proposed to describe the relationship between the roll compaction conditions and tablet strength, in which roll compaction was treated as a single, cumulative compaction step. They concluded that the relationship between the processes could be described by a single master compaction curve, referred to as a unified compaction curve. However, detailed validation was not carried out to determine the formulation compositional limits of the model.

Since it is of practical importance to predict the compression behaviour of pharmaceutical formulations during the complicated roll compaction process from a much simpler and rapid uniaxial compaction tests, the purpose of this study is to evaluate the accuracy of such predictions. It involves a comparison of the measured values of the pressure distribution in the nip region and those calculated from Johanson's model [3] for which the compression parameters are obtained from uniaxial compaction measurements. The pressure distributions are determined using an instrumented roll compactor with a gravity feed; consequently roll stresses arising from the feed region are assumed to be negligible. The study is an extension of that described by Bindumadhavan et al. [5] but under a wider range of operating conditions. In addition, the compression relationship used by Johanson [3] is extended so that it can describe pressures approaching zero. Inverse analyses of the measured pressure distributions are also carried out using a multivariate analysis to determine the values of the roll compression parameters for comparison with those obtained using uniaxial compaction.

2. Experimental

Microcrystalline cellulose (MCC) of Avicel-PH102 grade (FMC Biopolymer, USA) was selected as the model material. It is partially depolymerised alpha cellulose, which is prepared by reacting α-cellulose with mineral acids, producing needle-like particle shape. It is a white water insoluble, non-reactive and free flowing powder, and has an average particle size of 95–102 μm and a solids density of 1.52×10^3 kg/m^3. MCC has an effective angle of internal friction $\delta_E = 40.2^\circ$ and the wall friction angle (ϕ) with a stainless steel is 9.8°. The values were measured using a ring shear cell tester (Dietmar Schulze, Germany) with an applied normal stress of 8 kPa.

2.1. Uniaxial compaction

A universal testing machine (Lloyd 6000R, Lloyd Instruments Ltd., UK) with a 30 kN load cell was used to compress the powder. A cylindrical die of 13 mm internal diameter with a close fitting compression punch was used. Tablets corresponding to different feed aspect ratios (i.e., the ratio of initial bed height to bed diameter) were produced by adding pre-weighed powder to the die and tapping to obtain approximately reproducible packing. The initial powder bed height was recorded when contact was first made between the punch surface and powder; this involved using a greater gain for the load cell amplifier than that during compaction. Compaction was carried out at a rate of 5 mm/min to a maximum compaction force of 12 kN with five repeat measurements for aspect ratios in the range 0.63–1.25.

The data were fitted to the empirical compressibility relationship used by Johanson [3]:

$$\frac{\sigma}{\Sigma_\alpha} = \left(\frac{\rho}{\rho_\alpha}\right)^K \tag{1}$$

where σ and ρ are the current pressure and density of the powder, and K was termed as a compressibility constant. When Johanson applied this relationship to roll compaction, he ascribed Σ_α to the nip pressure without justification. Strictly it is actually a fitting parameter that defines the lower limit at which the relationship applies. The upper case symbols Σ_α and K are used to distinguish these fitting parameters from those for RC, for which the corresponding lower case symbols are used. The density ρ_α corresponds to that at the stress, Σ_α. The current density ρ is given by:

$$\rho = \frac{m}{\pi R^2 h} \tag{2}$$

where m is the mass of the powder, R is the internal radius of the die and h is the current height of the powder. Thus Eq. (1) can be written in the following form:

$$\ln\ \sigma = \ln\ \Sigma_\alpha + K \ln\left(\frac{h_\alpha}{h}\right) \approx \ln\ \Sigma_\alpha + K\tilde{\varepsilon} \tag{3}$$

where h_α is the height corresponding to Σ_α and

$$\tilde{\varepsilon} = \ln\left(\frac{h_\alpha}{h}\right) \tag{4}$$

is approximately the compressive natural strain. An equation of this form has been derived using a microscopic analysis [11]:

$$\ln\sigma = \ln[1 - \exp(-c\varepsilon)] + \ln\left(\frac{\tau_0}{c}\right) + c\varepsilon \tag{5}$$

where τ_0 is related to the mechanical strength of the particles and c is a microscopic pressure coefficient. As will be shown later, Eq. (5) can be written for RC be as

$$\ln\sigma = \ln[1 - \exp(-\kappa\varepsilon)] + \ln(\Sigma_\alpha) + \kappa\varepsilon \tag{6}$$

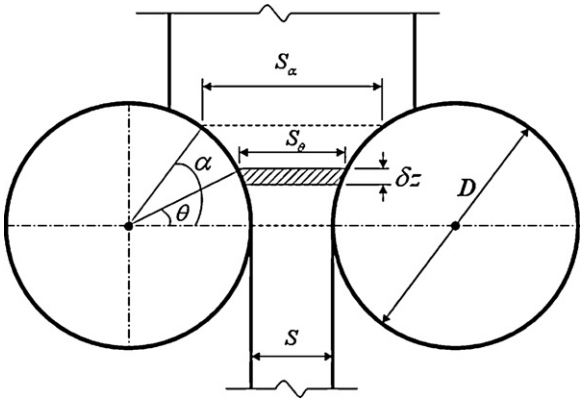

Fig. 2. Schematic diagram of a roll compactor showing the slabs that are parallel to the centre-to-centre axis of the rolls (assuming the neutral angle is at the minimum roll gap).

In this case

$$\varepsilon = \ln\left(\frac{h_i}{h}\right) \tag{7}$$

is the actual compressive natural strain, where h_i is the initial height of the powder. The inclusion of the first term in (6) allows data to be described at strains approaching zero.

2.2. Roll compaction

Roll compaction was carried out with a laboratory scale instrumented roll compactor that has been described previously [4,5,14]. The width and diameter of the rolls are 45 and 200 mm, respectively. Roll gaps of 0.9, 1.2, 1.4, 1.6 and 1.8 mm were investigated at roll speeds of 1–8 rpm; unless otherwise stated the term *roll gap* will imply the minimum gap between the two rolls and will be denoted as S. The powder was gravity fed to the rolls from a hopper. The initial volume of the feed powder was maintained constant by over-filling the hopper and levelling with a scraper. The angular position, θ, and the corresponding local roll pressure, σ_θ, were measured using a pressure transducer flush fitted in the centre of one of the roll surfaces. Data were collected at 0.18–0.56° intervals depending on the roll speed. They were analysed to derive the pressure distribution, i.e., the distribution of pressure at different angular positions as described by Bindumadhavan et al. [5].

The slab model [3] is now adapted to further analyse the pressure distribution data, in which an infinitesimal slab element with a constant thickness, δz, is considered to be compressed as the rolls rotate (see Fig. 2). This is different from that proposed by Johanson [3], in which a constant arc-length was assumed. Assume that the nip angle is defined relative to the minimum gap (i.e., the neutral angle is at the minimum roll gap) as adopted by Johanson [3] and then from Fig. 2 the length of the slab (i.e., the roll gap), S_θ, and the volume of the slab, V_θ, at any angle θ are given by:

$$S_\theta = S + D(1 - \cos\ \theta) \tag{8}$$

$$V_\theta = [1 + S^* - \cos\theta]\mathrm{DW}\,\delta z \tag{9}$$

where $S^* = S/D$ such that D and W are the diameter and width of the rolls. The length and the volume of the slab, S_α and V_α, at the lower stress limit σ_α, corresponding to the angle α, is as follows:

$$S_\alpha = S + D(1 - \cos\ \alpha) \tag{10}$$

$$V_\alpha = [1 + S^* - \cos\alpha]\mathrm{DW}\,\delta z \tag{11}$$

where the angle α is the apparent nip angle as defined by Johanson [3]. Consequently, using the pressure–density relationship (1) pro-

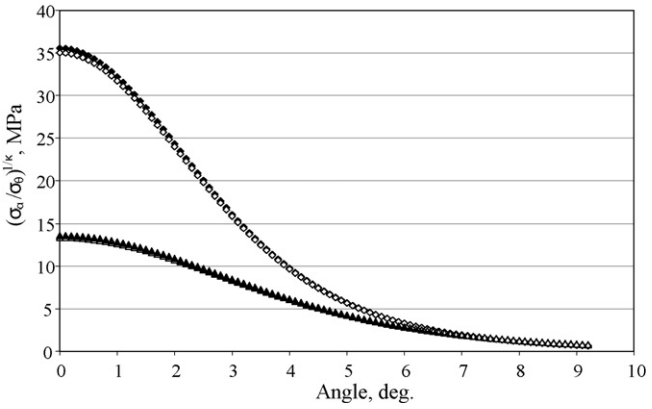

Fig. 3. The variation of $(\sigma_\theta/\sigma_\alpha)^{1/\kappa}$ with θ using Eqs. (12) and (15) for roll gap of 0.9 mm (♦, ◊) and 1.6 mm (▲, △), respectively (D = 200 mm).

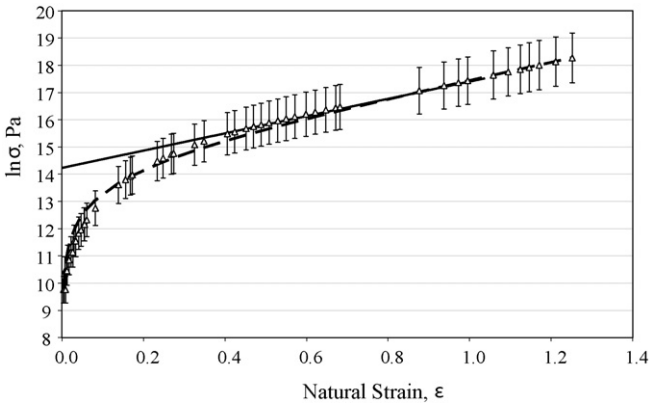

Fig. 4. Typical stress–strain data for uniaxial compaction (aspect ratio: 1.25); the solid line represents best fit to Eq. (3) and the dashed line shows the best fit to Eq. (5).

posed by Johanson [3], the measured stress normal to the surface of the roller, σ_θ, at an angle θ is given by:

$$\sigma_\theta = \sigma_\alpha \frac{\cos\alpha}{\cos\theta}\left[\frac{V_\alpha}{V}\right]^\kappa = \sigma_\alpha \frac{\cos\alpha}{\cos\theta}\left[\frac{1+S^*-\cos\alpha}{1+S^*-\cos\theta}\right]^\kappa \quad (12)$$

where σ_α is the lower limit of normal stress at which the equation applies. This equation is based on the compressive stress acting on a slab in a direction parallel to the centre-to-centre axis of the rolls, which at the angles θ and α is given by:

$$\widehat{\sigma}_\theta = \sigma_\theta \cos\theta \quad (13)$$

$$\widehat{\sigma}_\alpha = \sigma_\alpha \cos\alpha \quad (14)$$

This was not taken into account in Johanson's model [3], which was based upon the change in the volume of the slab and led to the following relationship:

$$\sigma_\theta = \sigma_\alpha \left[\frac{(1+S^*-\cos\alpha)\cos\alpha}{(1+S^*-\cos\theta)\cos\theta}\right]^\kappa \quad (15)$$

However, the numerical differences are relatively small since the maximum value of θ is typically small, as demonstrated graphically in Fig. 3.

Applying the slab model to roll compaction, Eqs. (4) and (7) can be written as:

$$\tilde{\varepsilon}_\theta = \ln\left(\frac{S_\alpha}{S_\theta}\right) = \ln\left[\frac{S+D(1-\cos\alpha)}{S+D(1-\cos\theta)}\right] = \ln\left(\frac{1+S^*-\cos\alpha}{1+S^*-\cos\theta}\right) \quad (0 \le \theta \le \alpha) \quad (16)$$

$$\varepsilon_\theta = \ln\left(\frac{S_\beta}{S_\theta}\right) = \ln\left(\frac{1+S^*-\cos\beta}{1+S^*-\cos\theta}\right) \quad (0 \le \theta \le \beta) \quad (17)$$

where κ and ε_θ are the compressibility constant and the natural strain for RC. S_β is the initial roll separation distance at the initial angle, β, where the stress is approximately zero since the powder is gravity rather than screw fed. That is, the angle β is defined as the value that corresponds to the roll gap, S_β and $\sigma_\beta \approx 0$. This angle β may be regarded as the true nip angle since it corresponds to the angle above which a finite normal stress is developed. It is reasonable to expect that for small increments in this angle there will be slip along the roll surface. At some angle $\beta' > \beta$, there will be a transition from slip to no-slip. In the current work, it will be assumed that $\beta' > \alpha$.

Thus, for roll compaction, Eqs. (3) and (6) may be written as:

$$\ln\widehat{\sigma}_\theta = \ln\widehat{\sigma}_\alpha + \kappa\tilde{\varepsilon}_\theta \quad (0 \le \theta \le \alpha) \quad (18)$$

$$\ln\widehat{\sigma}_\theta = \ln[1-\exp(-\kappa\varepsilon_\theta)] + \ln(\widehat{\sigma}_\alpha) + \kappa\varepsilon_\theta \quad (0 \le \theta \le \beta) \quad (19)$$

Substituting Eqs. (13), (14), (16) and (17) into Eqs. (18) and (19), we have

$$\ln\sigma_\theta = \ln\sigma_\alpha + \ln\left(\frac{\cos\alpha}{\cos\theta}\right) + \kappa\ln\left(\frac{1+S^*-\cos\alpha}{1+S^*-\cos\theta}\right) \quad (0 \le \theta \le \alpha) \quad (20)$$

$$\ln\sigma_\theta = \ln\left\{1-\exp\left[-\kappa\ln\left(\frac{S_\beta}{S_\theta}\right)\right]\right\} + \ln\sigma_\alpha + \ln\left(\frac{\cos\alpha}{\cos\theta}\right) + \kappa\ln\left(\frac{S_\beta}{S_\theta}\right) \quad (0 \le \theta \le \beta) \quad (21)$$

Eq. (20) can also be obtained from Eq. (12) directly.

3. Results and discussion

3.1. Uniaxial compression

Fig. 4 shows typical stress–strain data for uniaxial compaction with a feed aspect ratio of 1.25, in which the solid line represents the best fit to Eq. (3) and the dashed line shows the best fit to Eq. (5). The error bars are derived from three repeat runs. It is clear that Eq. (5) can be used to describe the entire data set but Eq. (3) can only fit the linear region at large strains. The fitting parameters Σ_α, the compressibility constant K, τ_0 and c are given in Table 1, in which those for uniaxial compaction at various feed aspect ratios are also presented. It may be seen that, as the feed aspect ratio increases, the compressibility constant K increases and Σ_α decreases. Nevertheless, the variation in the values of Σ_α, K, τ_0 and c for the different feed aspect ratios are relatively small and can be ascribed to the

Table 1
Parameters obtained from uniaxial compaction with various feed aspect ratios.

Aspect ratio	K	Σ_α (MPa)	c	τ_0 (MPa)	τ_0/c	α	β (0.9 mm)	β (1.6 mm)
0.63	2.74 ± 0.07	2.03 ± 0.12	2.54 ± 0.07	5.13 ± 0.17	2.03	7.4	7.5	7.8
0.95	3.07 ± 0.05	1.75 ± 0.03	3.07 ± 0.05	5.37 ± 0.16	1.75	7.0	7.1	7.3
1.25	3.17 ± 0.10	1.79 ± 0.23	3.17 ± 0.10	5.12 ± 0.57	1.79	6.8	6.9	7.1

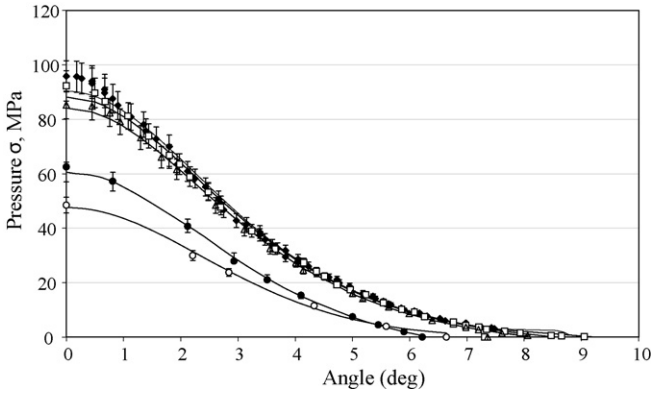

Fig. 5. The measured pressure distributions for a roll gap of 0.9 mm with the following roll speeds: 1 (♦); 2 (□); 3 (△); 6 (●) and 8 rpm (■). The lines are the best fit to the data using a multivariate analysis applied to Eq. (19) for obtaining optimal values of S_β, σ_β and κ.

influence of die wall friction. It is also interesting to note that, for the same aspect ratio:

$$c = K \tag{22}$$

and

$$\frac{\tau_0}{c} = \Sigma_\alpha \tag{23}$$

This can also be concluded by inspection of the terms in Eqs. (3) and (5). The value of the first term in Eq. (5) is small compared to the sum of the second and third terms even when $\sigma = \Sigma_\alpha$ and it tends to zero with increasing strain. Thus it is demonstrated that the inclusion of this term gives a more accurate representation of the stress–strain relationship when the strain approaches zero.

3.2. Roll compaction

Typical pressure distributions in the nip region during roll compaction are shown in Figs. 5 and 6. In these figures, the angle is set to be zero when the pressure reaches the maximum value; in practice the difference is less than 1 degree. Fig. 5 shows the pressure distributions at a roll gap of 0.9 mm for the various roll speeds considered. It is clear that the pressure increases as the angle decreases and reaches a maximum at the neutral angle. The maximum pressure decreases as the roll speed increases. This arises from entrained air that reduces the volumetric throughput of the feed powder and hence results in a reduction in the density at any roll angle. The

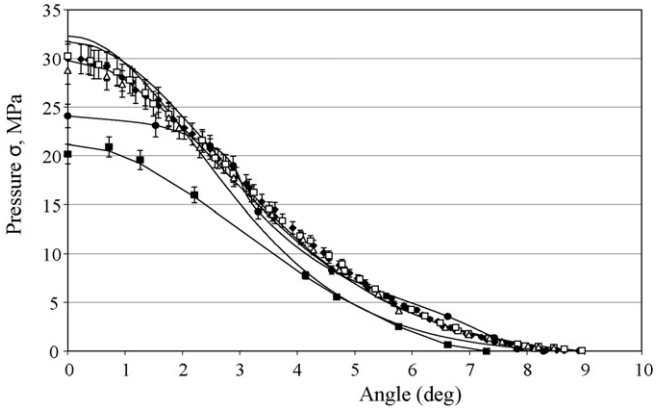

Fig. 6. The measured pressure distributions for a roll gap of 1.6 mm with the following roll speeds: 1 (♦); 2 (□); 3 (△); 6 (●) and 8 rpm (■). The lines are the best fit to the data using a multivariate analysis applied to Eq. (19) for obtaining optimal values of S_β, σ_β and κ.

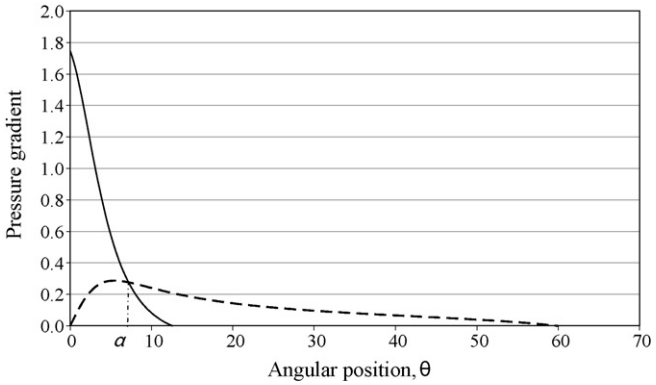

Fig. 7. Determination of the nip angle using Johanson's theory [3]. The dashed and solid lines were calculated from Eqs. (25) and (26).

corresponding pressure distributions as a function of roll speed at a roll gap of 1.6 mm are shown in Fig. 6. It can be seen that the maximum pressure increases with decreasing roll gap as would be expected from the increase in the uniaxial strain. These data are consistent with those reported previously [4,14,17].

It is of interest to explore if Eqs. (20) and (21) can be used to predict pressure distributions during roll compaction with the fitting parameters, σ_α and κ, obtained from uniaxial compaction measurements (i.e., with $\sigma_\alpha = \Sigma_\alpha$ and $\kappa = K$) since, for uniaxial compaction, the weight and the initial height of powder are known and the density at any applied strain can be calculated, so that the pressure–density relation can be accurately determined. While, for roll compaction, neither the density of the slab nor the nip angle is known. It is also clear from Eqs. (20) and (21) that, in order to predict the pressure distribution during roll compaction, the angles α and β have to be determined *a priori* even though σ_α and κ may be determined from uniaxial compaction measurements.

Johanson [3] proposed that the nip angle could be determined from the variation of the pressure gradients in the slip and nip regions since they are equal at the apparent nip angle (i.e., the apparent nip angle defines the transition from slip to no-slip boundary conditions):

$$\left(\frac{d\sigma}{dz}\right)_{slip} = \left(\frac{d\sigma}{dz}\right)_{nip} \tag{24}$$

The pressure gradient where no slip occurs along the roll surface is determined by differentiating Eq. (15) with respect to the roller position perpendicular to the centre-to-centre axis, thus:

$$\left(\frac{d\sigma}{dz}\right)_{nip} = \frac{\kappa\sigma_\theta(2\cos\theta - 1 - S^*)\tan\theta}{D/2(1 + S^* - \cos\theta)\cos\theta} \tag{25}$$

When slip occurs on the roll surface, the pressure gradient becomes:

$$\left(\frac{d\sigma}{dz}\right)_{slip} = \frac{4\sigma_\theta((\pi/2) - \theta - \nu)\tan\delta_E}{(D/2)[1 + S^* - \cos\theta][\cot(A - \mu) - \cot(A + \mu)]} \tag{26}$$

where

$$A = \frac{\theta + \nu + \pi/2}{2} \tag{27}$$

$$2\nu = \pi - \arcsin\frac{\sin\phi}{\sin\delta_E} \tag{28}$$

$$\mu = \frac{\pi}{4} - \frac{\delta_E}{2} \tag{29}$$

The intersection of the pressure gradient functions (Eqs. (25) and (26)) corresponds to the apparent nip angle as shown in Fig. 7, in which the curves are calculated using the frictional properties of

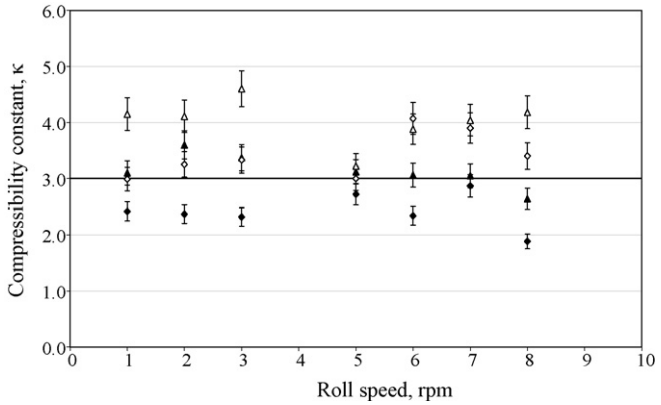

Fig. 8. The compressibility constant, κ, as a function of roll speed for two roll gaps, 0.9 (◊, ♦) and 1.6 mm (▲, △), determined from the fits shown in Figs. 5 and 6 with Eqs. (20) and (21), respectively. The line is the corresponding value of K.

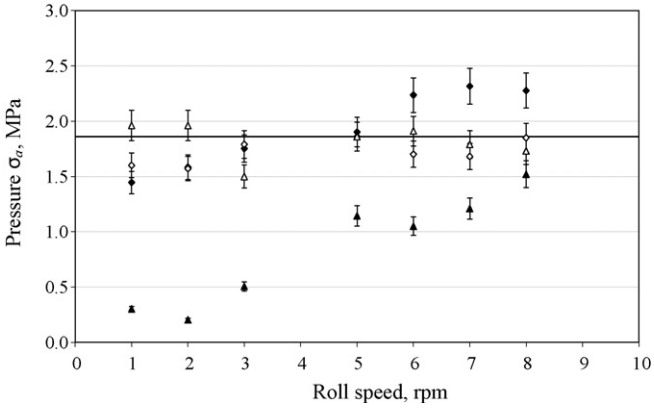

Fig. 9. The parameter σ_α as function of roll speed for two roll gaps, 0.9 (◊, ♦) and 1.6 mm (▲, △), determined from the fits shown in Figs. 5 and 6 with Eqs. (20) and (21), respectively. The line is the corresponding value of $\sum_a$.

MCC as given in Section 2. The calculated nip angles for the MCC is given in Table 1.

Since the boundary conditions for both Eqs. (20) and (21) are $\sigma = \sigma_\gamma$ when $\theta = \gamma = 0$, we have:

$$\left(\frac{S_\beta}{S_\alpha}\right)^\kappa \left\{1 - \exp\left[-\kappa \ln\left(\frac{S_\beta}{S}\right)\right]\right\} = 1 \tag{30}$$

Solving Eq. (30) for S_β, the angle β can then be determined. For the cases considered in the current study, the angle β at 0.9 and 1.6 mm roll gap for different values of κ are given in the last column of Table 1. It is clear that the $\alpha < \beta$ as expected. In the Johanson equation the value of α is essentially the lower limit to which the equation applies and moreover the apparent nip angle is independent of roll gap and roll speed. However, Eq. (6) is able to describe data at lower strains and therefore a more accurate prediction of true nip angle can be obtained.

3.3. Multivariate analysis of roll compaction

In this study, an inverse method with a multivariate analysis of the measured pressure distributions is adopted, in which multivariate fits of the pressure distributions during roll compaction under various process conditions are carried out and the parameters σ_α, κ, α and β can then be determined. The calculated values of σ_α and κ are then compared with the parameters Σ_α and K obtained from uniaxial compaction, in order to evaluate if uniaxial compaction measurements can be used to predict the roll compaction behaviour. The multivariate fits of Eq. (21) to the pressure distributions are also superimposed in Figs. 4 and 5. The calculated values of σ_α, κ, α and β are presented in Figs. 8–10.

Fig. 8 shows the variation of the RC compressibility constant κ with the roll speed at roll gaps of 0.9 and 1.6 mm (i.e., the minimum and maximum roll gaps considered). The compressibility constant K determined from uniaxial compaction for an average aspect ratio is also superimposed. It is clear that κ is relatively independent of roll speed and is generally comparable with the K determined from uniaxial compaction.

The variation of the pressure σ_α with roll speed and roll gap is shown in Fig. 9, in which the pressure Σ_α determined from uniaxial compaction for an average feed aspect ratio is also superimposed. It can be seen that the stress σ_α generally increases with roll speed and a smaller roll gap leads to a greater value of σ_α, which is as expected. However, the agreement between σ_α and Σ_α is only satisfactory for some combinations of roll speed and roll gap, indicating that σ_α is a sensitive parameter.

Fig. 10 shows the variation of the nip angles, α and β, obtained from the multivariate fits of Eqs. (20) and (21) with roll speed and roll gap, the average values of α and β predicted by the Johanson method [3] and Eq. (30) is also superimposed. It is clear that the nip angle decreases slightly as the roll speed increases, but it is relatively insensitive to the roll gap, which is in reasonable agreement with the analysis of Johanson [3]. The differences between α and β can be attributed to the relative fits of the equations to the measured pressure profiles. The inclusion of the first term in Eq. (21) allows the data to be fitted at relatively low strains hence giving a more accurate value for nip angle, which would be greater than the apparent value. Essentially, the value of α in Eq. (20) is strictly the lower limit to which the equation applies and rather than being the true nip angle.

3.4. Predicting roll compaction from uniaxial compaction measurements

Fig. 11 shows examples of the calculated pressure distributions using Eqs. (20) and (21) with the parameters (Σ_α and K) obtained from uniaxial compaction and the nip angle, α determined from Johanson's theory [3] and β determined using Eq. (30). The figure includes measured pressure distributions at roll speeds of 1 and

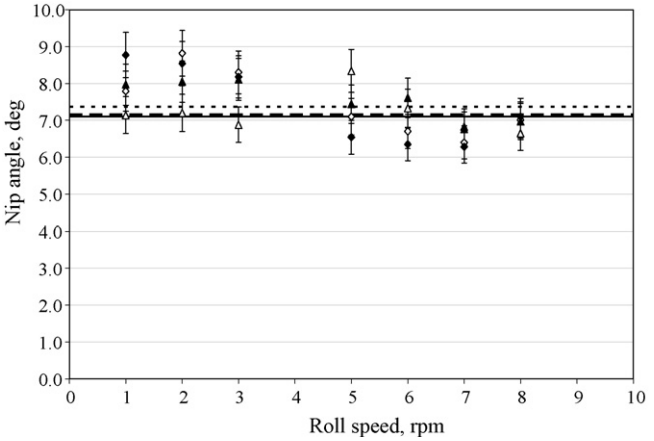

Fig. 10. The nip angle calculated from the parameter S_α and S_β as function of roll speed at two roll gaps, 0.9 (◊, ♦) and 1.6 mm (▲, △), determined from the fits shown in Fig. 4 with Eqs. (20) and (21), respectively. The solid line shows the apparent nip angle α determined using Eqs.(24)–(26), and the lines (■, ■)) shows the nip angle β calculated for roll gaps of 0.9 and 1.6 mm using Eq. (30), respectively.

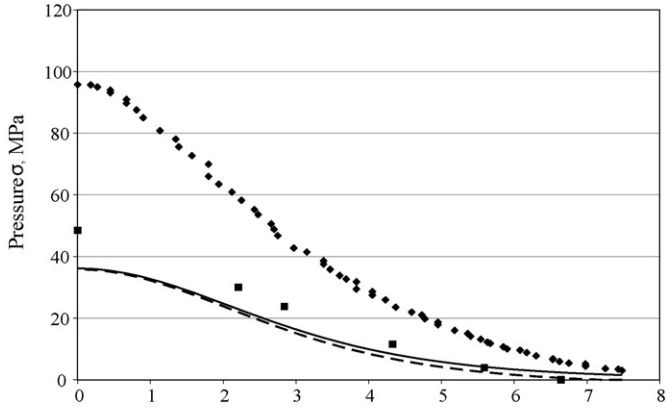

(a) Roll gap: 0.9 mm; roll speed 1rpm and 8 rpm.

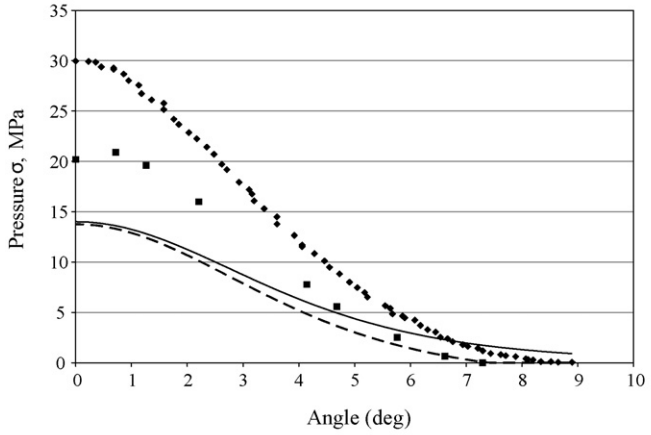

(b) Roll gap: 1.6 mm; roll speed 1 rpm and 8 rpm.

Fig. 11. Comparison of the calculated pressure distributions at roll speeds of 1 (♦) and 8 rpm (■) for different roll gaps. The lines (- - - , ...) show the predicted distributions calculated from Eqs. (20) and (21), respectively, using mean parameters determined from uniaxial compaction.

8 rpm with roll gaps of 0.9 mm (Fig. 11a) and 1.6 mm (Fig. 11b), the solid and dashed lines represent the predictions using Eqs. (20) and (21), only one curve can be used to predict the pressure distributions at any given roll gap as the models do not account for roll speed. It can be seen that, using the parameters determined from uniaxial compaction, both equations generally underestimate the pressure distribution during roll compaction. It is clear that the maximum pressure decreases as the roll speed increases, which is in excellent agreement with the observations reported in the literature [4,5,13,14]. The ratio of the measured and the calculated maximum pressures as a function of roll speed and roll gap is shown in Fig. 12. It can be seen that using the uniaxial compaction data, the maximum pressure distribution for RC is under-predicted by a factor 1.5–2.5, and the ratio of $\sigma_{max}^{(meas)}/\sigma_{max}^{(calc)}$ decreases as the roll speed increases, implying an improved agreement between measured and predicted maximum pressures can be obtained at higher roll speeds. This improvement arises because air entrainment becomes more important with increasing roll speed, as mentioned previously, which is not taken into account in the model. Thus the most direct comparison between the model and the experimental data is at small roll speeds.

The discrepancy between the measured and predicted pressure distributions may be attributed mainly to three factors: (1) it should be noted that the model treats roll compaction as a plane-strain problem (i.e., it is assumed that the compression

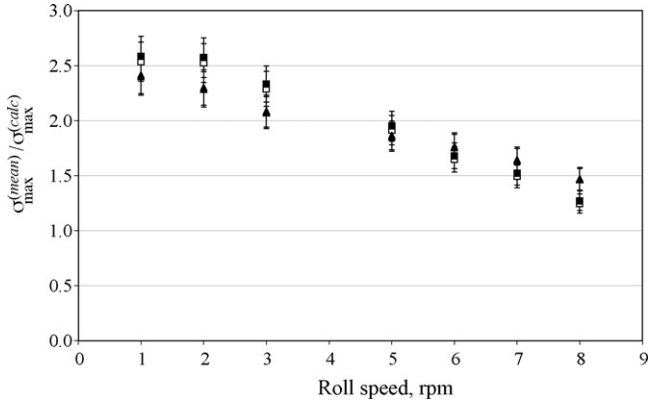

Fig. 12. The ratio of the maximum measured pressure to that calculated using Eqs. (20) and (21), $\sigma_{max}^{(meas)}/\sigma_{max}^{(calc)}$, as a function of roll speed at roll gaps of 0.9 mm and (□, ■) 1.6 mm (△, ▲), respectively, The calculations involved the mean parameters determined from UC at various aspect ratios (see Table 1).

pressure is uniform across the roll width). However, in the roll compaction experiments the pressure is measured using a sensor that is located in the centre of the roll width. Previous experimental work [1,14,19,20] showed that, for roll compaction with side cheek plates as the sealing mechanism as used in this study, the compression pressure across the roll width is not uniformly distributed. Instead, the pressure in the centre is greater than that at the edges. This is the result of the friction between the powder and the side cheek plates, which prevents the powder in the vicinity of the side cheek plates (i.e., near the edges of the roll) being drawn into the nip region [18,19] and thus leading to non-uniform powder feeding. Consequently, the measured pressure can be about 40% greater than the mean pressure across the rolls [20]. (2) Due to the non-uniform flow of powder in the nip region [19,20], a component of shear in the flow field will inevitably be induced due to the velocity being greater in the centre compared with that at the edges of the rolls. In addition, finite element analysis [20] demonstrated that across the ribbon thickness, the velocity in the centre of the ribbon was smaller than that at the roll surface, implying that shear was also induced along the ribbon thickness. However, during uniaxial compaction, the shear is essentially negligible. (3) It should be also noted that, in Johanson's model, the neutral angle was assumed to be coincident with the minimum roll gap, i.e., the maximum pressure was assumed to occur at the minimum roll gap and the offset of the neutral angle to the minimum gap [2,20] is ignored. This will underestimate the strain experience by the powder and consequently underestimate the maximum pressure.

4. Conclusions

The present study considers the pressure distributions developed during the roll compaction of microcrystalline cellulose (Avicel-PH102). An existing uniaxial compression relationship was adapted to describe the measured values. The advantage is that it is capable of being applied to low pressures. It has been found that uniaxial compaction is only a first order representation of a roll compaction process. In practice, the major factor is that the measured stress at the centre of the rolls is considerably greater than the mean value due to the non-uniform feeding of the feed powder. Moreover, there is a greater component of shear in the flow field due to the velocity being greater in the centre compared with that at the edges of the rolls, which is likely to cause a significant deviation from plug flow. In addition, it is possible that shear bands are formed during roll compaction. That is, uniaxial compaction represents a lower bound estimation since the redundant work is a significant fraction of the total work. Nevertheless, uniaxial com-

paction can be useful for comparing the maximum expected roll compaction pressures for a range of formulations and also evaluating tablets as prototype ribbons, provided that the maximum uniaxial compaction pressure is increased appropriately.

Acknowledgements

The authors would like to acknowledge the financial support of the Engineering and Physical Sciences Research Council, United Kingdom, through the EPSRC Engineering Doctorate Scheme in collaboration with Pfizer.

References

[1] Y. Funakoshi, T. Asogawa, E. Satake, Use of novel roller compactor with concave–convex roller pair to obtain uniform compacting pressure, Drug Development and Industrial Pharmacy 3 (1977) 555–573.
[2] W. Pietsch, Roll Pressing, Heyden and Son Ltd, London, 1976.
[3] J.R. Johanson, A rolling theory for granular solids, Journal of Applied Mechanics (1965) 842–848.
[4] F.R.G. Bourseul, Investigation on Roll Pressing as a Forming Operation, PhD Thesis, University of Birmingham (2001).
[5] G. Bindumadhavan, J.P.K. Seville, M.J. Adams, R.W. Greenwood, S. Fitzpatrick, Roll compaction of pharmaceutical excipient: experimental validation of rolling theory for granular solids, Chemical Engineering Science 60 (2005) 3891–3897.
[6] R.W. Miller, Advances in pharmaceutical roller compaction feed system design, Particle Technology European 6 (1994) 59–68.
[7] A. Gupta, G. Peck, R.W. Miller, K.R. Morris, Influence of ambient moisture on the compaction behaviour of MCC powder undergoing uni-axial compression and roller compaction: a comparative study using NIR, Journal of Pharmaceutical Sciences 94 (2005) 10.
[8] M.J. Adams, McKeown, Micromechanical analyses of the pressure volume relationships for powders under confined uniaxial compression, Powder Technology 88 (1996) 155–163.
[9] K. Kawakita, I. Hattari, M. Kishagami, Characteristic constants in Kawakita's powder compression equation, Journal of Powder and Bulk Solids Technology 1 (1977) 3–8.
[10] P.J. Denny, Compaction equations: a comparison of the Heckel and Kawakita equations, Powder Technology 127 (2002) 162–172.
[11] M.J. Adams, M.A. Muller, J.P.K. Seville, Agglomerate strength measurement using a uniaxial compaction test, Powder Technology 78 (1994) 5–13.
[12] Michel, PhD Dissertation, Contribution a l'etude de l'agglomeration des pourdres en presse a rouleaux lises, Universite de Compiegne, France, 1994.
[13] L.N.J. Perrea, Roll Compaction of Pharmaceutical Excipients, PhD Thesis, University of Birmingham, 2005.
[14] A.M. Miguelez-Moran, C.Y. Wu, J.P.K. Seville, The effect of lubrication on density distribution of roller compacted ribbons, International Journal of Pharmaceutics 362 (2008) 52–59.
[15] A.V. Zinchuk, M.P. Mullarney, B.C. Hancock, Simulation of roller compaction using a laboratory scale compaction simulator, International Journal of Pharmaceutics 269 (2008) 403–415.
[16] L. Farber, K.P. Hapgood, J.N. Michaels, F. Xi-Young, R. Meyer, M. Johnson, L. Feng, Unified compaction curve model for tensile strength of tablets made by roller compaction and direct compression, International Journal of Pharmaceutics 346 (2008) 17–24.
[17] K.A. Yehia, Estimation of roll press design parameters based on the assessment of a particular nip region, Powder Technology 177 (2007) 148–153.
[18] M.J. Adams, B.J. Briscoe, Tribology in Particulate Technology, Adam Higher, Bristol, 1987, p. 88.
[19] A.M. Miguelez-Moran, C.-Y. Wu, H. Dong, J.P.K. Seviller, Characterisation of density distributions in roller compacted ribbons using micro-indentation and X-ray micro-computed tomography, European Journal of Pharmaceutics and Biopharmaceutics 72 (2009) 173–182.
[20] J.C. Cunningham, Experimental studies and modelling of the roller compaction of pharmaceutical powders, PhD Thesis, Drexel University, 2005.